Surface-structure dependence of water-related adsorbates on platinum

Badan, C.

Chapter 6

The Interaction Between Water and Sub- and Pre-adsorbed Deuterium on Pt(211)

6.1 Abstract

We have studied the effects of pre- and post-dosing of deuterium on water desorption from (Pt[n(111)x(100)], n = 3), Pt(211), by temperature programmed desorption (TPD) experiments. Similar to other (100)-stepped Pt(111) surfaces with 4, 6, and 8 atom-wide terraces, Pt(211) with its 3 atom-wide terrace shows a maximum H-D exchange leading to HD and HDO formation at $\theta_{H_2O} < 0.5$ ML. The Pt(211) surface also becomes hydrophobic upon presaturating the surface with deuterium. A kinetic analysis of TPD spectra for a range of ultrathin water layer thicknesses shows that preadsorbed deuterium induces crystallinity over a larger range as compared to the bare Pt(211) surface. We explain this in terms of smoothening of the corrugation experienced by the first water layer. Similar studies using post-dosing of D_2 on adsorbed water layers does not seem to alter the H_2O structure as there is no detectable influence on the desorption energetics. Finally, we show that inherent (110)

kink defects in the (100)-type steps on this surface can be quantified by pre-deuterating the surface prior to water desorption. Their signature is especially useful when attempting to judge the surface quality without access to scanning probe techniques with (near) atomic resolution.

Based on: Badan, C.; Koper, M. T. M.; Juurlink, L. B. F., in preparation

6.2 Introduction

Water interfaces have become increasingly important for many areas of science particularly in electrochemistry[1, 2], astrophysics[3–5], chemistry[6, 7], biology[8] and physics[9, 10]. To reveal the underlying origins of the H_2O-metal interaction, adsorption of water onto metallic surfaces has been reviewed extensively over the past decades[11–13]. These studies highlight that the interfacial water structure depends, amongst other variables, on the adsorption temperature[14], substrate structure[15, 16], deposition technique[5], and the co-adsorbate[17, 18].

Platinum is considered a very good catalyst for several electrochemical reactions where interaction of water with the catalytic surface is relevant[19]. Prototypical surface science studies often use Pt(111) as a model to understand chemical and physical processes, such as adsorption, desorption, diffusion, occurring at the water-metal interface. Real catalytic surfaces, however, have a complex geometry with various types of defects such as kinks and steps. Because these defect sites increase the total reactivity of the surface especially for molecularly adsorbed species, the role of the steps and kinks in relation to water adsorption have gained more attention recently[16, 20–24]. Essentially, single atomic steps at surfaces control the formation of cubic ice (I_c) and hexagonal ice[7] (I_h) and enhance crystallinity[15, 16]. They affect long-range interaction in H_2O films and play a crucial role in wetting behaviour of the stepped Pt surfaces[23]. Although water preferentially adsorbs at the upper side of step edges[25], different H_2O structures, depending on the surface type, exist. For instance, water on Pt(553) wets the (110) step edges forming tetragons[21], whereas Pt(211) exhibits a zig-zag structure along its (100) step sites[26, 27].

Co-adsorption of water with hydrogen is particularly important in elucidating the chemistry taking place at the anode of low temperature fuel cells and the reversible hydrogen electrode[12, 13, 28]. Furthermore, the gas-surface interaction of H_2 with H_2O is critical in astrophysical environments because the physical and chemical properties of water play a crucial role in chemical and dynamical growth of the interstellar medium[17, 18]. Although numerous studies of water-metal interaction with various Pt model surfaces have been undertaken for decades, the co-adsorption of water and hydrogen on metallic surfaces has not received much attention.

In this study, we expand our knowledge of water-metal and gas-surface interactions using a highly stepped Pt surface with a very narrow (111) terrace, which has defect densities similar to actual nanoparticles. With high quality TPD measurements in combination with isotopic labeling, we study the effects of post-and-pre-deuteration on water desorption. Our results show the critical impact of the sequence of the D_2 exposure on the desorption energetics of water

and on the isotopic partitioning.

6.3 Experimental Section

Our equipment and the detailed procedures used for angle-resolved TPD experiments are discussed in detail elsewhere [15, 29]. Briefly, we performed our experiments using a home-built (UHV) system with a base pressure of 5×10^{-11} mbar. The chamber equips, amongst others, a differentially pumped quadrupole mass spectrometer (QMS, Baltzers QMA 400), a sputter gun (Prevac IS40C-PS), and LEED optics (VG RVL 900). Our samples are Pt single crystals prepared by Surface Preparation Laboratory, Zaandam, The Netherlands. They are 10 mm in diameter and 1-2 mm thick and have a purity better than 5N and an orientation better than 0.1^o. The polished side of the samples are cleaned under UHV conditions by repetitive sputtering and annealing cycles. During water (Milipore, 18.2 Ω) deposition, the sample is located at a fixed distance from the capillary array doser at T < 100 K. For the $H_2O/D_2/Pt(211)$ experiments, the cleaned surface is first exposed to D_2 by background dosing until the saturation coverage is reached. To lower the contamination by H or other residual gases, we start dosing at 700 K. For the $D_2/H_2O/Pt(211)$ experiments, first various amounts of water are dosed on the bare surface. Next, the surface is exposed to more than 250 Langmuir D_2 at < 100 K. For the TPD experiments, the heating rate was 0.92 Ks^{-1}. All our experiments are performed in the same UHV system with the same measurement conditions. We have also performed LEED experiments on Pt(211)[29]. The clean surface exhibits the expected diffraction pattern.

6.4 Results and discussion

Figure 6.1 displays H_2O TPD spectra from fully (1 ML) D_2 pre-covered Pt(211) at 0.9 Ks^{-1}. The dotted curve is 7.5 ML water desorbing from clean Pt(211). The inset figure shows more detailed spectra between 145 K - 165 K. The schematic shows three separate water layers, as indicated in orange, green and blue (same color-coding with the TPD spectra). Our previous studies[15, 29] showed that water cannot form hexagonal structures on bare Pt(211), (Pt[n(111)x(100)], n = 3) due to too narrow terrace sites. However, it can still build a 2D hydrogen-bonded network when adsorbed on Pt(211)[22, 26, 27]. When water desorbs from the bare Pt(211), TPD exhibits two peaks centered around 194 and 165 K. (dotted spectrum). The high and low temperature peaks are associated with the desorption from the (100) step sites and desorption from the second or subsequent water layers, respectively[30, 31].

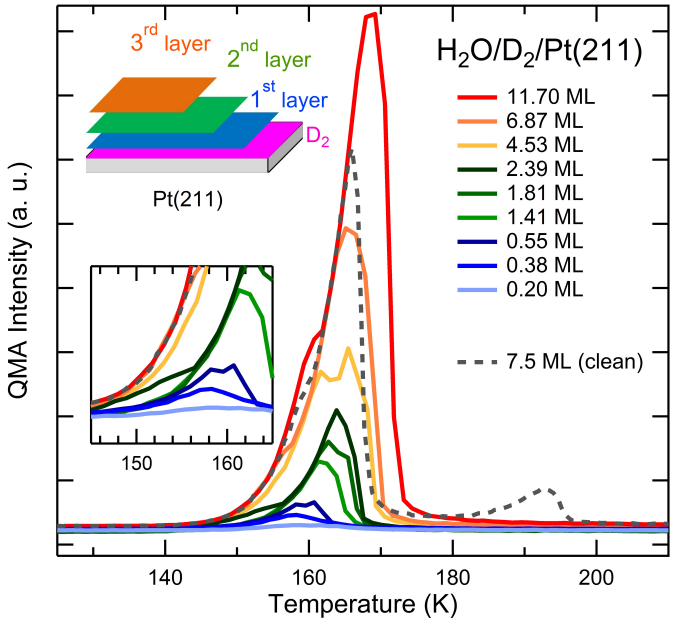

Figure 6.1: Water desorption from 1 ML D_2 pre-dosed Pt(211). The dotted curve shows water desorption from bare Pt(211). The inset figure shows the detailed spectra between 145 K and 165 K. The inset schematic illustrates the layer-by-layer growth of H_2O on the hydrogenated surface.

Water desorption from a fully hydrogenated Pt(211) appears in a broad, single desorption peak centered around 165 K, the same temperature as the water multilayer peak from the bare surface (dotted spectrum). We have previously shown that similar (100) stepped Pt(111) surfaces, (Pt[n(111)x(100)], n = 4, 6, and 8) also give rise to a nearly identical feature at this temperature[24, 32]. Following our previous studies[32], we attribute the single TPD peak to confined 3D water clusters near the step edge. Additionally, the spectra (between 0 and 12 ML) seem to have non-overlapping leading edges, but we note three different coverage regions (0 - 2 ML, 2 - 4.5 ML and 4.5 - 12 ML) for which the leading edges do overlap perfectly. At these coverage regimes, TPD shows zero-order desorption kinetics. The separation in the spectra suggests a layer-by-layer growth on the fully hydrogenated Pt(211) as illustrated in the inset schematic of figure 6.1. Later on, we provide a detailed kinetic analysis to shed light on the origin of these separated water layers.

Figure 6.2 shows traces of varying amounts of water desorbing from Pt(211)

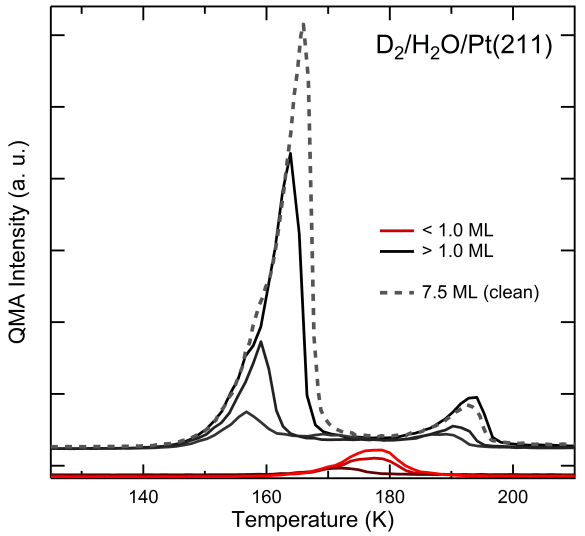

Figure 6.2: TPD spectra of increasing amounts of H_2O desorbing from 250 L D_2 post-dosed on Pt(211). The dotted spectrum is 7.5 ML of water desorbing from the bare surface.

onto which D_2 was dosed after H_2O dosing. To obtain these spectra, we exposed various amounts of H_2O to the clean surface at 95 - 100 K. Next, 250 L of deuterium were background dosed on the water covered surface at the same temperature. We confirm that 250 L of D_2 exposure on the bare Pt(211) is more than the amount which is enough to fully hydrogenate the surface under background dosing conditions[29]. The red and black spectra correspond to coverages of θ_{H_2O} < 1.0 ML and > 1.0, respectively. To show the clear difference in the spectra for coverages < 1.0 ML and > 1.0, we used different offsets. The dotted spectrum is 7.5 ML of H_2O desorbing from the clean surface. Below 1.0 ML of water coverage, the desorption from post-deuterated Pt(211) takes place in a single peak, centered below 180 K. In the sub-monolayer coverage regime, water desorption from clean Pt(211) appears at higher temperatures, 195 K[15, 29]. This significant temperature shift indicates that post-dosed D_2 lowers the binding energy for water. In our previous D_2 and H_2O co-adsorption study on Pt(533), Pt(755) and Pt(977)[32], we reported a similar behaviour. With increasing water exposure, the lowering effect in binding energy seems to vanish as the desorption peak at 180 K shifts to a higher temperature. Moreover, the TPD spectra look nearly identical to water desorption spectra from the clean surface (dotted spectrum) at higher water coverages.

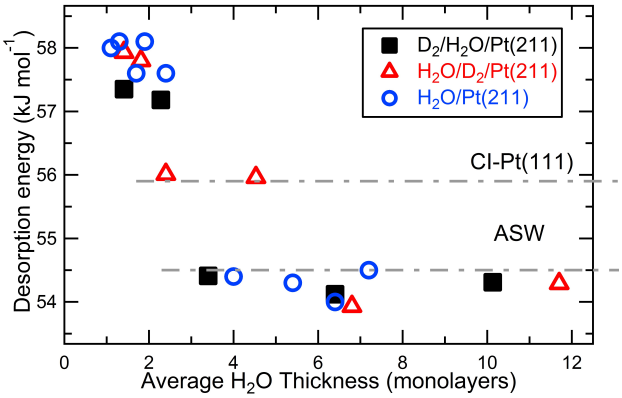

Figure 6.3: Energies of desorption at different water coverages. The red triangles and black squares indicate $H_2O/D_2/Pt(211)$ and $D_2/H_2O/Pt(211)$, respectively. The blue circles represent the E_d of water on a clean surface.

Although an ideal multilayer desorption feature displays an exponential increase in desorption rate with increasing temperature, the onsets of the H_2O multilayer desorption from clean, pre-hydrogenated and post-hydrogenated Pt(211) display a deflection at $\sim$ 156 K (figure 6.1 and 6.2). This deflection in the TPD spectrum below 170 K has previously been associated with crystallization of amorphous solid water (ASW) to crystalline ice (CI)[14, 15, 33, 34]. We have shown in chapter 5 in detail how very small differences in substrate structure influence crystallization of ultra thin water films significantly[15]. In the following section, we will show the role of co-adsorbed D on the crystallization of water on Pt(211).

Figure 6.3 illustrates the desorption energies (E_{des}) of H_2O as a function of water thickness. Water layer thicknesses are expressed in terms of our 1 $ML^{(111)}$ reference, as discussed in detail elsewhere[15]. The blue circles, black squares and red triangles represent $H_2O/Pt(211)$, $D_2/H_2O/Pt(211)$ and $H_2O/D_2/Pt(211)$, respectively. We obtained E_{des} by leading edge analysis[15]. The horizontal lines indicate the desorption energies of ASW and CI grown on Pt(111)[14, 33]. We note that our obtained E_{des} for ASW phase is ca. 1 kJ mol^{-1} lower than the reported values for thick water layers on Pt(111)[33, 35]. We believe that this minor difference may be associated with using a very narrow temperature regime to obtain the corresponding desorption kinetics. Nevertheless, our values indicate a clear difference between the water layers.

We have previously shown[15] that, when water is adsorbed below 100 K, CI-like and ASW layers grow on Pt(211) with desorption energies of 57.9 and 54.5 kJ

mol^{-1} (blue circles), respectively. For $D_2/H_2O/Pt(211)$, the obtained desorption energies are nearly identical to water desorption from the bare Pt(211). In both experiments crystallinity is maintained in the first two layers. This suggests the formation of very similar CI-like and ASW phases on bare and post-hydrogenated surfaces. On the other hand, for $H_2O/D_2/Pt(211)$ we note three different E_{des} at $\sim$ 57.8, 56.0 and 54.5 kJ mol^{-1}. This is also reflected on the TPD spectrum in figure 6.1. Because of distinct E_{des} obtained for three different water layers, TPD shows separated regimes between 0 - 2 ML, 2 - 4.5 ML and 4.5 - 12 ML. We attribute the calculated desorption energies for $H_2O/D_2/Pt(211)$ at 57.8 and 54.5 kJ mol^{-1} to CI-like and ASW phases, respectively. The obtained energies also suggest that CI-like formation is maintained in the first two layers similar to H_2O on the clean and post-deuterated Pt(211). However, between θ_{H_2O} = 2 - 5 ML, the desorption energy drops to 56 kJ mol^{-1}, signaling a different water phase. We note that this obtained E_{des} is identical to reported desorption energy of CI on Pt(111)[33, 35] (horizontal dotted lines in figure 6.3). Hence, we suggest that this phase is still crystalline. Finally, at $\theta_{H_2O} > 6$ ML, the E_{des} drops to 54.5 kJ mol^{-1} revealing the formation of ASW similar to water on clean and pre-deuterated Pt(211).

On D_2 pre-covered Pt(211), water grows crystalline in the first five layers (two layers as CI-like, three layers as CI). By comparison to clean and post-hydrogenated surfaces, the crystallinity is maintained over three additional layers on pre-hydrogenated surface. Picolin et al.[16] previously showed that highly corrugated surfaces suppress the formation of CI layers. Also in our previous study, we reported that crystallinity is maintained over a larger thickness on the less corrugated Pt surface[15]. Hence we suggest that pre-deuterating the surface introduces a smoothening effect to the corrugated surface.

To elucidate to what extent the sequence of the co-adsorbed D_2 influences the isotopic exchange, we show the isotopic partitioning of HD and HOD from the D_2 and H_2O co-adsorption experiments as a function of H_2O coverage in figure 6.4. The data in this figure are obtained by monitoring HD and HOD desorption rates during our TPD experiments as shown in figure 6.1 and 6.2. The top and middle panels show the isotopic exchange of HD and HOD, respectively. The bottom panel displays the absolute amounts of D_2 desorbing from post-and-pre-deuterated Pt(211). Our preliminary H_2O and D_2 experiments on clean Pt(211) showed no desorption traces of HD and HOD. Hence, the obtained coverages are only due to the isotopic exchange between H_2O and D_2. The red data points correspond to water dosed onto D_2 pre-covered Pt(211), $H_2O/D_2/Pt(211)$, and the black data points indicate the water dosed onto D_2 post-covered Pt(211), $D_2/H_2O/Pt(211)$. The dotted lines fitted through the data are only a guide for

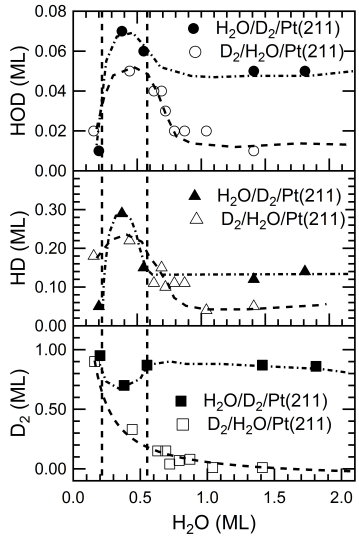

Figure 6.4: The top and middle panels show isotopic partitioning of HOD and HD as a function of water coverage, respectively. The bottom panel shows D_2 coverage. The solid (red) and empty (black) markers indicate $H_2O/D_2/Pt(211)$ and $D_2/H_2O/Pt(211)$, respectively. The lines fitted to the data are only a guide for the eye.

the eye.

We observe that both $H_2O/D_2/Pt(211)$ and $D_2/H_2O/Pt(211)$ give rise to a maximum amount of HOD and HD exchange at $\theta_{H_2O} \approx 0.4$ ML. On a fully deuterated Pt(533), Pt(755), and Pt(977) the maximum isotopic partitioning is also obtained at a nearly identical coverage[32, 36]. The combined results suggest that the HD and HOD exchange on a fully deuterated Pt is not influenced by the terrace length.

In our co-adsorption experiments, we observe two distinct behaviours for deuterium desorption (bottom panel in figure 6.4). For $D_2/H_2O/Pt(211)$, the amount of deuterium desorbing ($D_{2,des}$) from Pt(211) decreases with water coverage, $\theta_{H_2O} < 1.0$ ML. Under these conditions deuterium adsorption seems only achievable when water does not wet the entire surface. This agrees with the lack of significant isotopic exchange for the $D_2/H_2O/Pt(211)$ system at $\theta_{H_2O} > 1.0$ ML. On the other hand, when reversing the desorption order, $H_2O/D_2/Pt(211)$, the $D_{2,des}$ from Pt(211) is nearly 1.0 ML and hardly drops with prolonged water exposure. The adsorbed water molecules does not displace the dissociated D_{ad} on the surface. In addition, in figure 6.5, we show the TPD spectra of D_2 and H_2O

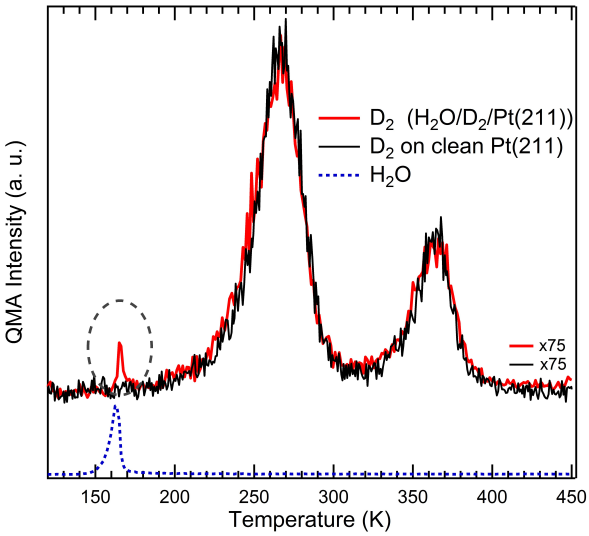

Figure 6.5: TPD spectra of D_2 (red) and H_2O (blue) for $\theta_D = 1.0$ ML pre-dosed on Pt(211). The black spectrum is 1.0 ML of D_2 desorbing from clean surface[29]. The dotted, grey circle shows the early D_2 desorption as a result of trapping.

desorbing from pre-deuterated Pt(211). We have previously shown the deuterium desorption from Pt(211) in chapter 4. Briefly D_2 desorption takes place in two peaks. The high and low temperature peaks are attributed to desorption from (100) steps and (111) terraces, respectively. For $H_2O/D_2/Pt(211)$, the D_2 spectrum (red spectrum) gives an additional peak, which is not observed when D_2 is dosed on the clean Pt(211) (black spectrum), at 160 K. Note that the onset of the water desorption (blue dotted spectrum) coincides with the desorption of this additional D_2. The desorption intensity of this feature, which corresponds to $\sim$0.01 ML of D_2, does not increase with prolonged water exposure.

Smith et al. have observed a similar desorption feature for CCl_4 desorption on water post-dosed Au(111). They attributed this peak to the nucleation and growth of CI from ASW[37]. For $H_2O/D_2/Pt(211)$, the peak at 160 K cannot signal the crystallization because water is already crystalline in the first five layers, as shown in (figure 6.3). Furthermore, theoretical[38] and astrophysical[39] studies for D_2 desorption show that hydrogen may bind chemically, but without dissociation, near steps at < 50 K. In this study, as mentioned earlier, we dose D_2 on the bare surface at significantly higher temperatures, 95 - 100 K. Therefore molecular D_2 cannot be trapped by the post-dosed H_2O to give a delayed desorption feature at 160 K.

Van der Niet et al.[24] have also reported a similar D_2 desorption feature on a water post-covered Pt(553), Pt[4(111)x(110)], at 163 K. Unlike H_2O/D_2/Pt(211), this peak grows in intensity as a function of water coverage and delays the onset of deuterium desorption feature. They suggested that this peak is associated with H_2O adsorbing on the (110) steps. Once the water, adsorbed on these (110) step sites, starts to desorb, the underlying D_{ad} can desorb as well. Although Pt(211) is only supposed to have three atom wide (111) terraces truncated by (100) steps, the actual sample contains (110) steps as defect sites too. Following van der Niet et al.[24], we associate the peak at 160 K with the D_2 desorption from the (110) step defects on Pt(211). Therefore, the integral of the D_2 peak at 160 K, 0.01 ML, reflects the absolute amount of (110) step defects, 1 %, present on the crystal. Their occurrence may be due to both a minor azimuthal miscut of the crystal and their entropically required presence for a perfectly stepped crystal at temperatures well above T = 0 K. Figure 6.6 shows the schematic representation of the (110) step defects on a Pt(211) crystal. The arrows indicate the sites, introduced by these defects. These defects clearly have different adsorption sites than the regular (100) step sites. The dissociated D_{ad} can adsorb onto these defect sites and give rise to the desorption feature at 160 K, as shown in figure 6.5.

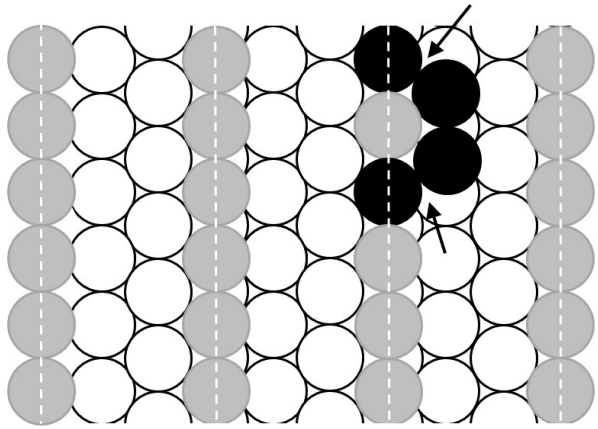

Figure 6.6: Schematic representation of a Pt(211) crystal with (110) step defects. The arrows indicate the (110) step defects that give rise to the desorption feature at 160 K as shown in figure 6.5.

6.5 Conclusion

In conclusion, we have shown that H_2O adsorbed on post- and pre-hydrogenated Pt(211) have markedly different characteristics. Fully deuterating the surface prior to water adsorption makes Pt(211) hydrophobic, similar to other (100) stepped Pt(111) surfaces with n = 4, 6, and 8. Post-deuteration does not change the wetting behaviour of the surface but lowers the binding energy of water at $\theta_{H_2O} < 1.0$ ML. Both co-adsorption experiments yield the maximum isotopic partitioning at the sub-monolayer water coverages. Furthermore, the desorption kinetics have been studied systematically for different water coverages. We find that post-deuteration of the surface does not influence crystallization kinetics of water. However, pre-deuteration of the highly corrugated surface introduces a smoothening effect. This effect introduces an additional CI phase, that is not observed when H_2O is adsorbed on clean or post-hydrogenated surface. Additionally, crystallization of water on pre-hydrogenated Pt(211) is maintained over a double thickness by comparison to water on clean and post-hydrogenated surface. Finally, we have shown that (110) step defects on pre-deuterated Pt[n(111)x(100)] samples can be revealed to an extent as low as 1 % or lower. We believe that our results give new insights into water-metal and gas-surface reactions taking place on metal surfaces, in particular concerning the crystallinity of water layer layers in dependence of the structural and chemical nature at the underlying substrate.

6.6 Bibliography

References

(1) Filhol, J.-S.; Neurock, M. *Angewandte Chemie International Edition* **2006**, *45*, 402–406.

(2) Rossmeisl, J.; Nørskov, J. K.; Taylor, C. D.; Janik, M. J.; Neurock, M. *The Journal of Physical Chemistry B* **2006**, *110*, 21833–21839.

(3) Nisini, B. *Science* **2000**, *290*, 1513–1514.

(4) Kouchi, A. *Nature* **1987**, *330*, 550–552.

(5) Mayer, E.; Pletzer, R. *Nature* **1986**, *319*, 667–674.

(6) Stevenson, K. P.; Kimmel, G. A.; Dohnalek, Z; Smith, R. S.; Kay, B. D. *Science* **1999**, *283*, 1505–1507.

(7) Thürmer, K.; Nie, S. *Proceedings of the National Academy of Sciences of the United States of America* **2013**, *110*, 11757–11762.

(8) Baldwin, R. L. *Science* **2002**, *295*, 1657–1658.

(9) Fecht, H. J. *Nature* **1992**, *356*, 133–135.

(10) Carrasco, J.; Hodgson, A.; Michaelides, A. *Nature materials* **2012**, *11*, 667–674.

(11) Hodgson, A.; Haq, S. *Surface Science Reports* **2009**, *64*, 381–451.

(12) Henderson, M. A. *Surface Science Rep.* **2002**, *46*, 1–308.

(13) Thiel, P. A.; Madey, T. E. *Surface Science Reports* **1987**, *7*, 211–385.

(14) Löfgren, P; Ahlström, P; Chakarov, D. *Surface Science* **1996**, *367*, L19–L25.

(15) Badan, C.; Heyrich, Y.; Koper, M. T. M.; Juurlink, L. B. F. *The Journal of Physical Chemistry Letters* **2016**, 1682–1685.

(16) Picolin, A.; Busse, C.; Redinger, A.; Morgenstern, M.; Michely, T. *The Journal of Physical Chemistry C* **2009**, *113*, 691–697.

(17) Amiaud, L; Fillion, J.; Baouche, S; Dulieu, F; Momeni, A; Lemaire, J. *The Journal of chemical physics* **2006**, *124*, 094702.

(18) Fillion, J.-H.; Amiaud, L.; Congiu, E.; Dulieu, F.; Momeni, A.; Lemaire, J.-L. *Physical Chemistry Chemical Physics* **2009**, *11*, 4396–4402.

(19) Koper, M. T. M. *Nanoscale* **2011**, *3*, 2054–2073.

(20) Fajín, J. L. C.; D. S. Cordeiro, M. N.; Gomes, J. R. B. *The Journal of Physical Chemistry A* **2014**, *118*, 5832–5840.

(21) Kolb, M. J.; Farber, R. G.; Derouin, J.; Badan, C.; Calle-Vallejo, F.; Juurlink, L. B. F.; Killelea, D. R.; Koper, M. T. M. *Physical Review Letters* **2016**, *116*, 136101.

(22) Peköz, R.; Wörner, S.; Ghiringhelli, L. M.; Donadio, D. *The Journal of Physical Chemistry C* **2014**, *118*, 29990–29998.

(23) Den Dunnen, A.; van der Niet, M. J. T. C.; Koper, M. T. M.; Juurlink, L. B. F. *Journal of Physical Chemistry C* **2012**, *116*, 18706–18712.

(24) Van der Niet, M. J.; den Dunnen, A.; Koper, M. T.; Juurlink, L. B. *Physical review letters* **2011**, *107*, 146103.

(25) Morgenstern, M; Michely, T; Comsa, G *Physical Review Letters* **1996**, *77*, 703–706.

(26) Endo, O.; Nakamura, M.; Sumii, R.; Amemiya, K. *Journal of Physical Chemistry C* **2012**, *116*, 13980–13984.

(27) Nakamura, M.; Sato, N.; Hoshi, N.; Soon, J. M.; Sakata, O. *Journal of Physical Chemistry C* **2009**, *113*, 4538–4542.

(28) Roman, T.; Groß, A. *Catalysis today* **2013**, *202*, 183–190.

(29) Badan, C.; Koper, M. T. M.; Juurlink, L. B. F. *The Journal of Physical Chemistry C* **2015**, *119*, 13551–13560.

(30) Grecea, M. L.; Backus, E. H. G.; Riedmuller, B; Eichler, A; Kleyn, A. W.; Bonn, M *Journal of Physical Chemistry B* **2004**, *108*, 12575–12582.

(31) Gee, A. T.; Hayden, B. E. *The Journal of Chemical Physics* **2000**, *113*, 10333–10343.

(32) Den Dunnen, A.; van der Niet, M. J. T. C.; Badan, C.; Koper, M. T. M.; Juurlink, L. B. F. *Physical Chemistry Chemical Physics* **2014**, 8530–8537.

(33) Smith, R. S.; Matthiesen, J.; Knox, J.; Kay, B. D. *Journal of Physical Chemistry A* **2011**, *115*, 5908–5917.

(34) Backus, E. H. G.; Grecea, M. L.; Kleyn, A. W.; Bonn, M. *Physical Review Letters* **2004**, *92*, 236101–236104.

(35) Löfgren, P.; Ahlström, P.; Lausma, J.; Kasemo, B.; Chakarov, D. *Langmuir* **2003**, *19*, 265–274.

(36) Van der Niet, M. J. T. C.; Dominicus, I.; Koper, M. T. M.; Juurlink, L. B. F. *Physical Chemistry Chemical Physics* **2008**, *10*, 7169–7179.

(37) Smith, R. S.; Huang, C; Wong, E.; Kay, B. D. *Physical review letters* **1997**, *79*, 909.

(38) McCormack, D. A.; Olsen, R. A.; Baerends, E. J. *The Journal of chemical physics* **2005**, *122*, 194708.

(39) Hornekær, L.; Baurichter, A.; Petrunin, V. V.; Luntz, A. C.; Kay, B. D.; Al-Halabi, A *The Journal of chemical physics* **2005**, *122*, 124701.